Piloted Evaluation of Flying-V with Incremental Nonlinear Dynamic Inversion and Envelope Protection

Atmaca, D.; Stroosma, O.; van Kampen, E.

DOI
10.2514/6.2025-0973

Publication date
2025

Document Version
Final published version

Published in
Proceedings of the AIAA SCITECH 2025 Forum

AIAA SciTech Forum
6-10 January 2025, Orlando, FL
AIAA SCITECH 2025 Forum

10.2514/6.2025-0973

Piloted Evaluation of Flying-V with Incremental Nonlinear Dynamic Inversion and Envelope Protection

Direnc Atmaca*, Olaf Stroosma†, and Erik-Jan van Kampen‡
Delft University of Technology, Kluywerweg 1, 2629 HS, Delft, The Netherlands

The Flying-V is a novel flying wing aircraft design that aims to improve aerodynamic efficiency and fuel consumption. In recent years, there has been an increased effort to evaluate the handling qualities (HQs) of the Flying-V, and to develop new flight control strategies. One of the latest flight control designs for the Flying-V uses Incremental Nonlinear Dynamic Inversion (INDI) with a Flight Envelope Protection system. The purpose of this research is to validate this FCS design and its conclusions on handling qualities by conducting piloted experiments. To facilitate a sound comparison, the aerodynamic model, flight control structure, and airframe characteristics are taken as is from the existing study. For the experiment, numerous maneuvers are designed and carried out. The experiment is performed on the SIMONA Research Simulator of the Delft University of Technology, with three real-life test pilots as participants. The results show a significant correlation with offline findings and demonstrate the improvement in HQs provided by the flight control system.

I. Introduction

The conventional commercial aircraft that consists of a fuselage and two wings has been dominating the market for the last 50 years [1]. Lately, with an increase in strong public opinion on environmental protection, the efficiency requirements for aircraft have been becoming increasingly stringent. As a result, this drove aircraft designs to have higher fuel efficiency, less noise, and larger capacity. However, the fuel efficiency of the conventional design has been approaching an asymptote since the 1980s. To overcome this stagnation in fuel efficiency, some new airframe concepts such as blended-wing-body (BWB) and flying-wing have been proposed. One promising flying-wing design that was initially proposed by Benad [2] is called the Flying-V. It is a long-distance energy-efficient commercial aircraft concept that integrates passengers, cargo hold, and fuel tanks inside two merged wings, creating a unique V shape*. The Flying-V promises significant improvements in aerodynamic efficiency and up to 20% fuel savings compared to Airbus A350-1000, all while managing to keep the same wing span with a shorter length [2–4].

Since its conception, Flying-V has been gaining increasing attention from the research community. Over the last ten years, many studies have been published focusing on a variety of design aspects, including model identification, control systems, aerodynamic analysis and optimization, and assessment of handling qualities (HQ). An important component of Flying-V research is the design of the flight control system (FCS) and the evaluation of the handling qualities. The Flying-V flight control problem is a challenging one due to the distinctive design of the airframe. In recent years, many studies have focused on identifying, understanding, and solving a range of flight control problems related to the Flying-V model. An earlier paper pointed out that the Flying-V has pitch-break tendencies when the angle of attack is greater than 19 degrees, leading to static instability [5]. Another study on handling qualities revealed that the Dutch roll is insufficiently damped and is highly coupled with other dynamic modes [6]. Recent piloted simulator experiments have investigated these issues related to the model [7–9]. The experiments assessed the handling qualities of the Flying-V through pilot feedback, with each study examining different stability components under different flight conditions and aircraft configurations. This revealed the need for refining the aircraft model and the control system. Consequently, as the Flying-V evolves, handling quality assessment stands to be a major part of the research and is also imperative for certification.

Most recently, three papers focusing on modeling, control, and handling qualities have been published [10–12]. These papers present three important contributions for handling quality analysis and control system design of the Flying-V. The first is aerodynamic modeling using data generated with a Vortex Lattice Method (VLM) and data from

*PhD Candidate, Control and Simulation, Faculty of Aerospace Engineering, AIAA Student Member
†Senior Researcher, Control and Simulation, Faculty of Aerospace Engineering, Senior AIAA Member
‡Associate Professor, Control and Simulation, Faculty of Aerospace Engineering
*https://www.tudelft.nl/en/ae/flying-v

previous wind tunnel experiments (WTE), performed on a scaled Flying-V model. Since VLM is a linear method, it cannot capture nonlinear phenomena. For this reason, VLM is used as a baseline model, where it is expanded using the WTE data to include nonlinearities. The second contribution is an offline handling quality analysis focusing mainly on the dynamic modes for both bare and augmented airframe models. The results of the offline analysis verified many of the previous findings, such as the insufficiently damped Dutch roll. In addition, it created a baseline handling quality expectation that needs to be validated through pilot-in-the-loop experiments. Lastly, the third contribution is the design of an Incremental Nonlinear Dynamic Inversion (INDI) flight controller [13–16] that uses a law based on the C* parameter [17, 18] for longitudinal control, a roll rate command for lateral control, and a sideslip compensator for directional control. In addition, the control system is equipped with a flight envelope protection (FEP) system with angle of attack, bank angle, and load factor limits. Compared to previous control designs for the Flying-V, INDI is a big step forward as it is more robust against uncertainties in aerodynamic coefficients, and it only requires an onboard control effectiveness model to derive the control law.

To carry the Flying-V research even further, a Flying-V Flight Control Project is currently underway. The project aims to increase the Technology Readiness Level (TRL) of the Flying-V control systems from 3 to 5, while ensuring level 1 handling qualities for the augmented airframe and level 2 for the bare-airframe. To this end, several developments are being made in aerodynamic model identification, scaling, and control system design and evaluations.

This paper presents four research contributions. The first is validating the handling quality findings detailed in [10, 11]. The second contribution is validating the non-piloted simulation results of the INDI flight control system with FEP proposed in [12]. The third contribution is to demonstrate that FCS reduces pilot workload and leaves an overall impression of safety on the pilots. The last contribution is to test whether the FEP functionality works as intended and prevents the aircraft from exceeding the designated limits.

To accomplish these through piloted handling quality evaluations, three pilots are invited as participants. As simulation platform, the SIMONA Research Simulator (SRS) [19] of Delft University of Technology (TU Delft) is used. SRS is a sophisticated simulator equipped with a flight deck, motion system, visual display system, and control loading system. The pilots are asked to perform a variety of longitudinal and lateral-directional maneuvers specifically chosen for proper HQ evaluation. The results are collected using the Cooper-Harper rating scale [20], PIO rating scale [21], EASA CS-25 Easy Access Rules [22], and verbal pilot feedback.

The structure of this paper is as follows: Section II covers the aircraft modeling, including a discussion of the aerodynamic model, physical parameters, and control surface specifications. Section III explains the control allocation and the system setup for the bare-airframe as well as the INDI-based flight control system. Section IV outlines the expected handling qualities that resulted from the offline analyses in previous studies. Section V discusses the setup of the experiment in the SRS, the tasks given to the pilots, the flight conditions, the pilot qualifications and the experiment timeline. Section VI describes the results and provides a detailed discussion. Finally, Section VII gives an overview of the paper, outlines the main findings, and suggests future directions for the research.

II. Aircraft Modeling

The Flying-V is under continuous development, which means that there have been many design iterations of the airframe. As a result, there is great variability between each iteration, resulting in different structural characteristics, control surface layouts, aerodynamic models, and flight conditions. This paper uses the aircraft model described in [10, 11].

A. Aerodynamic Model

The aerodynamic model is a combination of two models identified through different methods. The first is the linear VLM model, which is obtained from another study [6]. Due to its linear nature, VLM is limited in accurately representing the entire flight envelope. The validity of the model degrades as the point of evaluation moves away from the predetermined flight conditions. The model is only considered to be valid for angle of attack values between -5 to 15 degrees. In addition, the model does not consider other factors such as the landing gear model, compressibility, ground effect, aeroelasticity, and atmospheric effects.

From previous research, the Flying-V is known to have pitch break tendencies at higher angle of attack values [5, 6]. The pitch break is inherently nonlinear and cannot be captured using a linear model. For this reason, a second model identified from wind tunnel experiments (WTE) is used [23]. However, the WTE model also has limitations due to the setup of the experiment. The wind tunnel experiments are performed on a subscale half-span model of the Flying-V [5], leading to lower fidelity. Also, since measurements are taken with sensors that are placed along the wingspan, they are

affected by structural vibrations. During model identification, the wingtips that contain the rudders were removed from the analysis, making it quite difficult to identify lateral-directional behavior. This also makes it challenging to capture Dutch roll characteristics from nonlinear data.

To combine these two models, the VLM is used as a baseline, where its longitudinal coefficients are modified using the wind tunnel data to capture the pitch-break behavior. However, there are some important points that must be considered before combining the models. Firstly, the control surface layout between the subscale model used in WTE and the full-scale model used in VLM is different. The subscale model has no rudders but has three elevons on each wing, whereas the full-scale model has one rudder and two elevons on each side. In addition, the subscale coefficients must be scaled up before they can be integrated with the full-scale coefficients.

Considering that the WTE model cannot be used to capture the Dutch roll, the lateral direction coefficients C_Y, C_L, and C_N are directly taken from the VLM model. For the remaining coefficients, C_X, C_Z, and C_M are combined using both models. For angle of attack values between -5 and 15 degrees, they are taken from the VLM, and between 15 and 30 degrees, they come from the WTE model. Using the combined model, the aerodynamic coefficients are determined for cruise (M = 0.85) and approach (M = 0.2) conditions. Figures 1 and 2 show the longitudinal coefficients in these conditions for the combined and separate models.

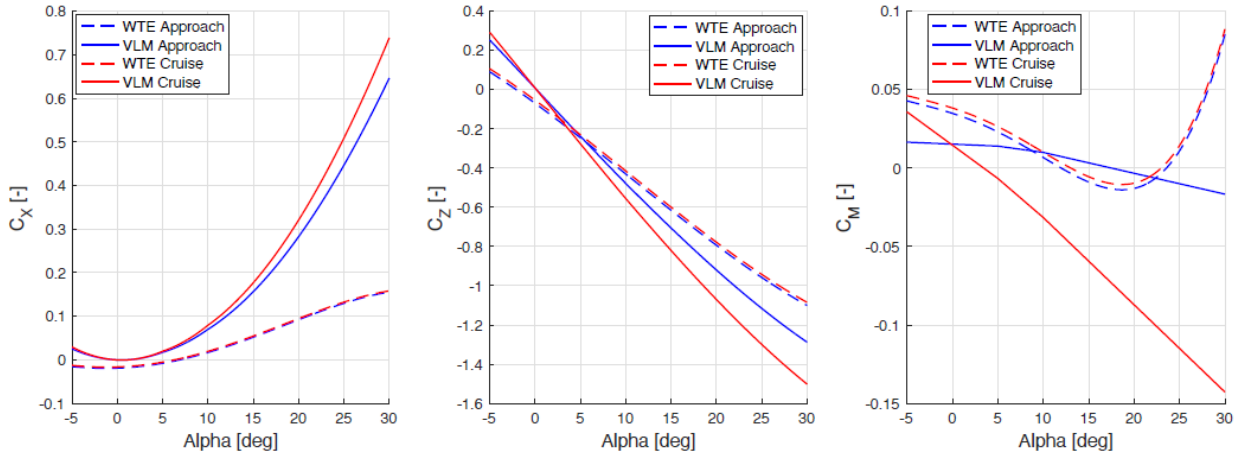

Fig. 1 Longitudinal coefficients for WTE and VLM in cruise and approach conditions, taken from [10]

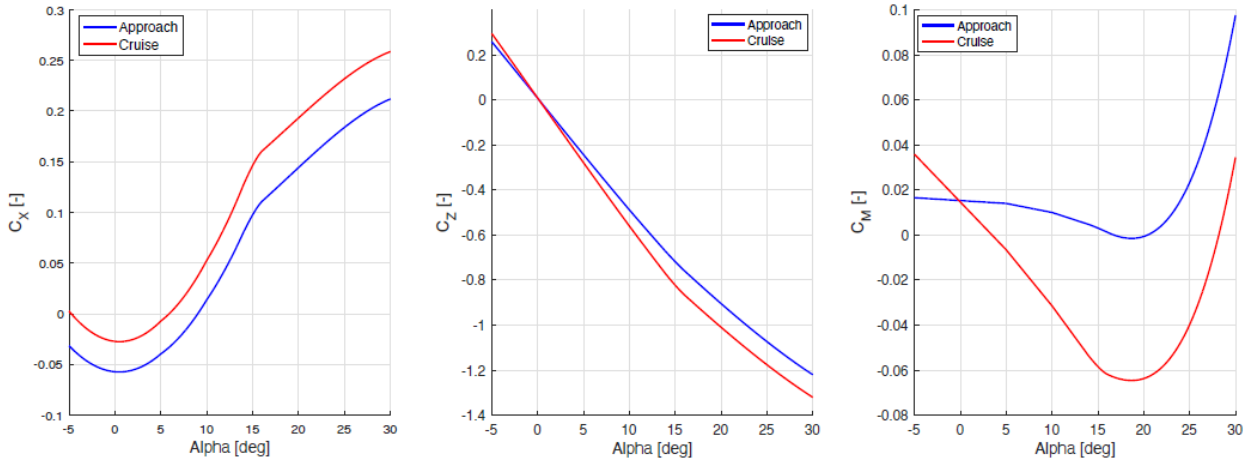

Fig. 2 Longitudinal coefficients for the combined model, taken from [10]

From the pitching moment figure C_M, it can be seen that when considered separately, VLM cannot capture pitch break. However, the combined model is able to capture this in both cruise and approach conditions.

B. Aircraft Configuration

The structural and physical parameters of the airframe are taken from Cappuyns [6]. These values are also used by van Overeem [10, 11] for aerodynamic model construction and offline handling quality analysis. The layout of the control surfaces is given in Figure 3. The current Flying-V configuration possesses two elevons and one rudder on each side. The rudders are controlled with a single control input; hence, they are considered as a single control surface. The control surface deflection rate limits are taken from Stougie [12], whereas the deflection range comes from [6]. The definitions of the control surfaces and limits are given in Table 1.

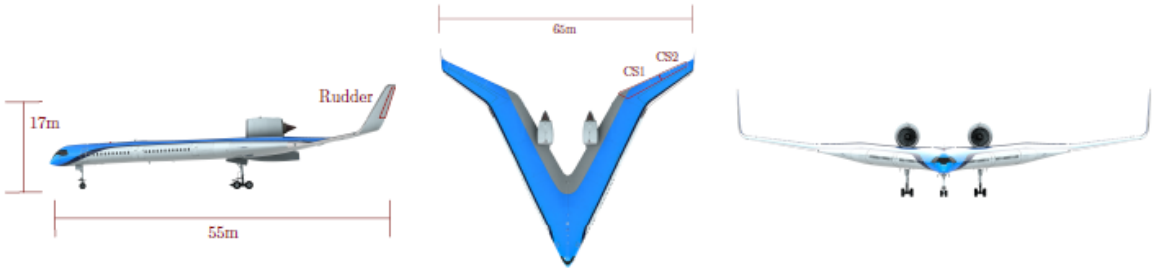

Fig. 3 Control surface layout, obtained from [11]

The aircraft configuration is chosen in a way that allows validating the offline handling quality analysis of both the bare airframe and the augmented airframe through piloted evaluations. The next section focuses on the distinction between the bare and augmented airframe, and explains the method of augmentation.

Table 1 Control surfaces and corresponding limits, based on [6, 12]

Label	Control Surface	Deflection Range, deg	Deflection Rate Range, deg/s
$CS1_L$	Left inboard elevon	[-25,25]	[-80,80]
$CS2_L$	Left outboard elevon	[-25,25]	[-80,80]
$CS1_R$	Right inboard elevon	[-25,25]	[-80,80]
$CS2_R$	Right outboard elevon	[-25,25]	[-80,80]
CS3	Rudders	[-30,30]	[-120,120]

III. Flight Control System

This section explains the bare and augmented airframe models, as well as the associated control allocation. For both airframes, the structural parameters, control surface deflection limits, aerodynamic model, and actuator dynamics are kept the same. The dynamics of the aircraft, sensors, and actuators are directly taken from the control design proposed in [12], which originates from [24].

A. Bare-airframe Model

Bare-airframe refers to aircraft with no stability augmentation system. In this configuration, the pilot directly commands the control surfaces using the sidestick for longitudinal and lateral channels, and through the pedals for directional. Figure 4 shows the setup of the bare-airframe. In the figure, u stands for the control input that results from control allocation, x is the aircraft state vector, and x_{meas} is the measured aircraft state vector including the effect of sensor noise on the states. Actuator dynamics are modeled as second-order systems. The control allocation used for the bare-airframe is referred to as explicit-ganging in the literature. With this method, the relationship between the pilot input and the control input is fixed. The pilot inputs are spread over the elevons and rudders manually. The relation for

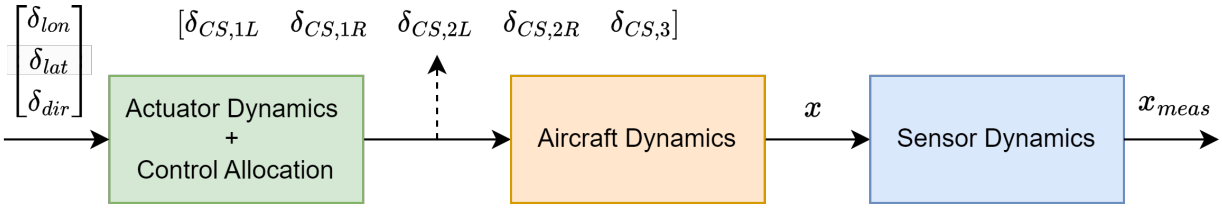

Fig. 4 Bare-airframe setup

control allocation is given in 1.

$$\begin{bmatrix} \delta_{CS,1L} \\ \delta_{CS,1R} \\ \delta_{CS,2L} \\ \delta_{CS,2R} \\ \delta_{CS,3} \end{bmatrix} = \begin{bmatrix} 0 & -1 & 0 \\ 0 & -1 & 0 \\ 1 & -1 & 0 \\ -1 & -1 & 0 \\ 0 & 0 & -1 \end{bmatrix} \begin{bmatrix} \delta_{lon} \\ \delta_{lat} \\ \delta_{dir} \end{bmatrix} \tag{1}$$

In equation 1, δ_{CS} stands for the control surface deflections, and $\delta_{lon,lat,dir}$ are the longitudinal, lateral, and directional pilot inputs, respectively. Since the Flying-V has an unconventional airframe, control allocation is not straightforward. In traditional aircraft, there is a clear distinction between control surfaces such that ailerons are used only for lateral motion and elevators for longitudinal motion. However, the Flying-V has four elevons that act as both elevator and aileron. This requires the designer to make a decision about the control allocation. For the purposes of this study, all elevons are used for longitudinal control, whereas only the outboard elevons are used for lateral control.

B. Augmented-airframe Model

The discussion is divided into two parts, the inner loop and the outer loop. The inner loop covers the control allocation and the derivation of Incremental Nonlinear Dynamic Inversion, whereas the outer loop contains the C* controller, the roll and pitch reference models, sideslip compensator, pseudo-control hedging, linear controller, and the flight envelope protection system. An overall schematic of the control system is shown in Figure 5.

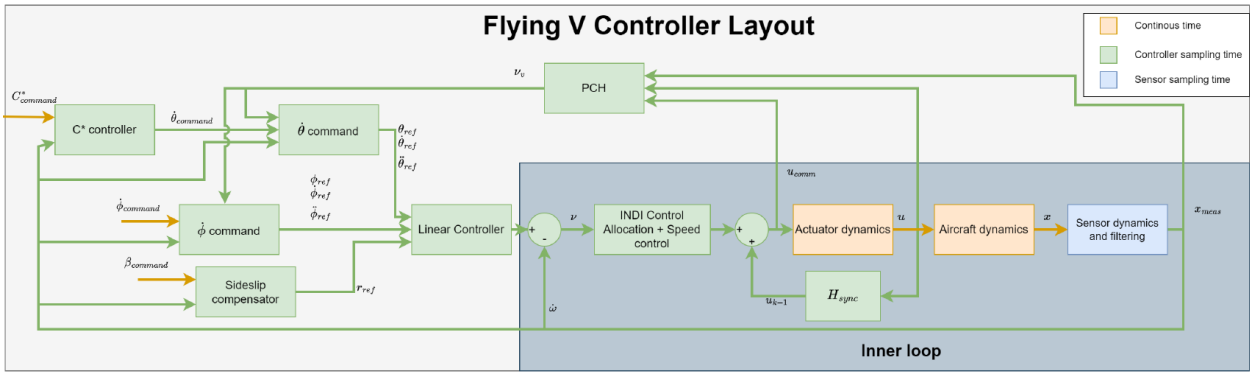

Fig. 5 Flight Control System Layout, obtained from [12]

1. Inner Loop

The control system used for the augmented airframe is based on incremental nonlinear dynamic inversion (INDI), which is fundamentally a sensor-based feedback linearization method. By linearizing the system through model inversion, INDI allows using linear control methods such as PID for flight control. Assuming the system is control-affine, it can be written as in equation 2.

$$\dot{\boldsymbol{x}} = f(\boldsymbol{x}) + G(\boldsymbol{x})\boldsymbol{u} \quad \text{and} \quad \boldsymbol{y} = h(\boldsymbol{x}) \tag{2}$$

In equation 2, $\boldsymbol{x}$ refers to the state vector, $\boldsymbol{u}$ is the input vector, and $\boldsymbol{y}$ is the output vector. Starting from this control-affine system, it is possible to apply Taylor expansion while neglecting higher-order terms. Applying the expansion leads to equation 3.

$$\begin{aligned}\dot{\boldsymbol{x}} &\approx \dot{\boldsymbol{x}}_0 + \frac{\partial}{\partial \boldsymbol{x}}\left[f(\boldsymbol{x}) + G(\boldsymbol{x})\boldsymbol{u}\right]_{\boldsymbol{u}_0,\boldsymbol{x}_0}(\boldsymbol{x}-\boldsymbol{x}_0) + \frac{\partial}{\partial \boldsymbol{u}}\left[f(\boldsymbol{x}) + G(\boldsymbol{x})\boldsymbol{u}\right]_{\boldsymbol{u}_0,\boldsymbol{x}_0}(\boldsymbol{u}-\boldsymbol{u}_0) \\ &= \dot{\boldsymbol{x}}_0 + \frac{\partial}{\partial \boldsymbol{x}}\left[f(\boldsymbol{x}) + G(\boldsymbol{x})\boldsymbol{u}\right]_{\boldsymbol{u}_0,\boldsymbol{x}_0}(\Delta\boldsymbol{x}) + G(\boldsymbol{x}_0)(\Delta\boldsymbol{u})\end{aligned} \tag{3}$$

To simplify this expression even further, we can use the time-scale separation principle. Assuming that the control derivatives are much larger than the state derivatives, it is possible to rewrite this as in equation 4.

$$\boldsymbol{u} = \boldsymbol{u}_0 + G^{-1}(\boldsymbol{x}_0)(\boldsymbol{\nu} - \dot{\boldsymbol{x}}_0) \tag{4}$$

In this equation, $\boldsymbol{\nu}$ is the virtual control input that comes from a linear controller. The incremental nature of the equation is apparent as the control input of the current step, $\boldsymbol{u}$, results from an incremental update on $\boldsymbol{u}_0$. Also, as a result of the time-scale separation, calculating the control input only requires the control effectiveness terms of the aerodynamic model contained in $G(\boldsymbol{x}_0)$, where its complete form is given in equation 5.

$$G(\boldsymbol{x}_0) = \frac{\rho V^2 Sc}{2}\boldsymbol{I}^{-1}\begin{bmatrix} C_{l_{\delta_{CS1L}}} & C_{l_{\delta_{CS1R}}} & C_{l_{\delta_{CS2L}}} & C_{l_{\delta_{CS2R}}} & C_{l_{\delta_{CS3}}} \\ C_{m_{\delta_{CS1L}}} & C_{m_{\delta_{CS1R}}} & C_{m_{\delta_{CS2L}}} & C_{m_{\delta_{CS2R}}} & C_{m_{\delta_{CS3}}} \\ C_{n_{\delta_{CS1L}}} & C_{n_{\delta_{CS1R}}} & C_{n_{\delta_{CS2L}}} & C_{n_{\delta_{CS2R}}} & C_{n_{\delta_{CS3}}} \end{bmatrix} \tag{5}$$

From equation 4, it is clear that this matrix has to be inverted. However, since the Flying-V has five control surfaces and only three moments need to be controlled, the control effectiveness matrix is not square; hence, it cannot be directly inverted. To overcome this issue, a proper control allocation strategy must be employed. For this reason, the method of Cascaded Generalized Inverses (CGI) [25] is preferred. This strategy uses the Moore-Penrose pseudo-inverse for the inversion while minimizing the overall control surface deflections. In case of control saturation, the algorithm removes the rows and columns related to the saturated control surface from the control effectiveness matrix and re-allocates the controls over the surfaces. This is repeated until no saturated control surfaces remain. For the complete algorithm and details regarding the CGI, the reader is referred to [12, 25].

2. Outer Loop

Fundamentally, the outer loop defines the interaction between the pilot input and the inner loop controller. This is done by defining control laws that convert the pilot inputs into roll, pitch, and yaw commands or references that must be followed by the aircraft.

For longitudinal control, the FCS uses an Airbus-inspired C* approach. The C* is a criterion that combines load factor and pitch rate, where the load factor dominates at higher speeds and the pitch rate at lower speeds. Essentially, with this controller, the pilot commands a C* parameter through longitudinal sidestick inputs. The input then goes into the longitudinal controller to generate a pitch rate command, $\dot{\theta}_{com}$. The command in turn is sent to a pitch reference model to create pitch, pitch velocity, and pitch acceleration references to be used by the linear controller. In addition, the C * controller block seen in Figure 5 contains a load factor and angle of attack protection (AoA). The load factor, by default, is limited to the range -1.0 to 2.5. The angle of attack protection works as a modifier of the maximum and minimum load factor values, where the maximum AoA changes between 22 and 24 degrees depending on altitude, and the minimum is set to -5 degrees. To modify the load factor limits, the current AoA is subtracted from the maximum and minimum AoA, and the result is multiplied by a gain. These results are then sent to “min” and “max” statements to find the load factor protection limits. The AoA protection is disabled when the AoA of the aircraft is between 0 and 15 degrees to prevent interference within the standard operational boundaries. The structure of the C* controller and the protection systems are available in [12].

The lateral control implemented in the FCS is quite similar to the C* controller. The pilot commands roll rates through lateral sidestick inputs. This input is sent to a roll reference model, which acts as a second-order filter to generate roll, roll velocity, and roll acceleration references for the linear controller. Also, the reference model includes a roll protection scheme. Roll values are limited to the range between -66 and 66 degrees. Lastly, for directional control, the FCS includes a sideslip compensator. For this, the pilot directly commands sideslip angles through pedal inputs. The input is then converted into a yaw rate reference, r_{ref}.

All these reference signals generated by the roll and pitch reference models as well as the sideslip compensator must be followed by the aircraft. The generated signals are sent to a linear controller that utilizes a proportional-integral (PI) scheme to calculate a control input for the body rates ν_p, ν_q, and ν_r that stabilizes the error dynamics. After this, the measured angular rates $\dot{p}$, $\dot{q}$, and $\dot{r}$ are subtracted from the control inputs to obtain the final virtual control that is sent to the inner loop.

An important feature of the FCS discussed in this section is the Pseudo Control Hedging (PCH), which is a method to create protection against control saturation. PCH calculates a virtual hedge, $\boldsymbol{\nu}_h$, using the difference between actual and commanded control surface deflections. This control input is then subtracted from the roll and pitch acceleration references in each model, which essentially scales the commanded control deflections to a level achievable by the actuators.

The next section will focus on presenting the offline handling quality results from previous studies for the bare and augmented airframe, as well as providing a brief discussion about the tuning of the FCS.

IV. Handling Quality Expectations

This section explains the analytical handling quality expectations for the bare and augmented airframe. The results presented in this section are taken from a series of papers that illustrate the gradual progress of the Flying-V control system [10–12]. Since the focus of this paper is to perform a piloted handling quality validation of the existing bare-airframe model and the flight control system, the most direct approach is comparing the simulator results with these analytical expectations.

A. Bare-airframe Analytical Handling Qualities

This study uses three types of handling quality requirements, which are the trim requirements from EASA CS-25 [22], modal requirements from MIL-F-8785C [26], and the Control Anticipation Parameter (CAP). For comparison purposes, only the modal and CAP requirements will be taken into account, as these allow for direct classification of handling qualities between level 1 and 3. The offline analysis is limited to only approach and cruise conditions.

1. Modal Analysis Results

The MIL-F-8785C document [26] outlines several frequency and damping requirements for dynamic modes of the aircraft. To calculate these modal values, the aircraft must first be linearized at its trim condition. After expressing the linearized system in state-space form, the eigenmodes of the linearized system can be directly calculated from the system matrix A. These eigenmodes for the approach and cruise conditions are given in Tables 2 and 3.

Table 2 Eigenmodes for the approach condition at the forward and aft CG, obtained from [10]

	Approach (M = 0.2)							
	Forward CG				Aft CG			
Eigenmodes	ζ	ω	T_r, s	T_s, s	ζ	ω	T_r, s	T_s, s
Short Period	0.683	0.681	-	-	0.744	0.609	-	-
Phugoid	$-2.31 \cdot 10^{-3}$	0.161	-	-	$-4.37 \cdot 10^{-2}$	0.146	-	-
Dutch Roll	$-8.14 \cdot 10^{-2}$	0.992	-	-	$-8.97 \cdot 10^{-2}$	0.848	-	
Aperiodic Roll	-	-	1.26	-	-	-	1.32	-
Spiral	-	-	-	42.6	-	-	-	79.4

The handling quality levels for these values can be obtained by comparing them with the requirements defined in [26]. In these tables, ζ stands for the damping ratio, ω is the natural frequency, T_r is the roll time constant in seconds, and T_s is the spiral time constant in seconds. Before moving on with the exact requirements for each mode, it would make sense to explain the meaning of flying/handling quality levels.

Flying quality levels according to MIL-F-8785C:

- Level 1: Flying qualities clearly adequate for the mission flight phase
- Level 2: Flying qualities adequate to accomplish the mission flight phase, but some increase in pilot workload or degradation in mission effectiveness, or both, exists
- Level 3: Flying qualities such that the airplane can be controlled safely, but the pilot workload is excessive or mission effectiveness is inadequate, or both

Now that the definitions are established, the requirements for each eigenmode are given in Table 4.

Table 3 Eigenmodes for the cruise condition at forward and aft CG, obtained from [10]

	Cruise (M = 0.85)							
	Forward CG				Aft CG			
Eigenmodes	ζ	ω	T_r, s	T_s, s	ζ	ω	T_r, s	T_s, s
Short Period	0.225	2.01	-	-	0.303	1.41	-	-
Phugoid	$7.19 \cdot 10^{-2}$	$5.43 \cdot 10^{-2}$	-	-	$6.97 \cdot 10^{-2}$	$5.37 \cdot 10^{-2}$	-	-
Dutch Roll	$-7.38 \cdot 10^{-3}$	0.811	-	-	$4.68 \cdot 10^{-3}$	0.732	-	
Aperiodic Roll	-	-	1.32	-	-	-	1.71	-
Spiral	-	-	-	Stable	-	-	-	Stable

Table 4 Modal requirements for the approach and cruise conditions, based on [10, 26]

Modes	Levels	Approach (M = 0.2)	Cruise (M = 0.85)
Short Period	Level 1	$0.5 < \zeta_{sp} < 1.3$	$0.3 < \zeta_{sp} < 2.0$
	Level 2	$0.35 < \zeta_{sp} < 1.3$	$0.2 < \zeta_{sp} < 2.0$
	Level 3	$0.25 < \zeta_{sp}$	$0.1 < \zeta_{sp}$
Phugoid	Level 1	$0.04 < \zeta_{sp}$	$0.04 < \zeta_{sp}$
	Level 2	$0 < \zeta_{sp}$	$0 < \zeta_{sp}$
	Level 3	Unstable with $55s < T_{sp}$	Unstable with $55s < T_{sp}$
Dutch Roll	Level 1	$\zeta_d > 0.08 \quad \zeta_d\omega_d > 0.10 \quad \omega_d > 0.5$	$\zeta_d > 0.08 \quad \zeta_d\omega_d > 0.10 \quad \omega_d > 0.5$
	Level 2	$\zeta_d > 0.02 \quad \zeta_d\omega_d > 0.05 \quad \omega_d > 0.5$	$\zeta_d > 0.02 \quad \zeta_d\omega_d > 0.05 \quad \omega_d > 0.5$
	Level 3	$\zeta_d > 0 \quad \omega_d > 0.4$	$\zeta_d > 0 \quad \omega_d > 0.4$
Aperiodic Roll	Level 1	$T_r < 1.4s$	$T_r < 1.4s$
	Level 2	$T_r < 3.0s$	$T_r < 3.0s$
	Level 3	$T_r < 10.0s$	$T_r < 10.0s$
Spiral	Level 1	$T_s > 17.3s$	$T_s > 28.9s$
	Level 2	$T_s > 11.5s$	$T_s > 11.5s$
	Level 3	$T_s > 7.2s$	$T_s > 7.2s$

By comparing the eigenmode values of the bare-airframe model given in Tables 2 and 3, with the requirements defined in 4, it is possible to obtain the handling or flying quality classifications. Looking at the short period at the aft center-of-gravity, the bare-airframe has Level 1 handling qualities in both cruise and approach conditions, whereas at the forward CG, it has Level 2 in both flight conditions. For the phugoid during approach, the eigenvalues indicate instability since their real component is positive. Hence, the approach condition cannot be classified using the MIL-F-8785C standard. However, during the cruise, both aft and forward CG locations exhibit Level 1 handling qualities. Dutch roll is mostly unstable and cannot be classified, except at the aft CG for cruise condition, where it shows Level 3 handling qualities. Aperiodic roll is stable for all CG locations and flight conditions. For the approach condition, it displays Level 1 handling qualities, while for the cruise it shows Level 1 at the forward CG and Level 2 at the aft CG. The spiral mode is stable at the cruise condition, which automatically puts it in the Level 1 category; however, it is unstable during the

approach. Even though the mode is unstable, the handling quality category depends on the spiral time constant, which puts it at Level 1 for the approach at both CG locations.

Overall, although this might not be the case for all modes, the forward CG is less stable than the aft. Hence, for the control augmentation and the associated piloted evaluations, only the forward CG will be studied, as it is more critical than the aft CG.

2. Control Anticipation Parameter

The control anticipation parameter (CAP) is mainly a longitudinal parameter concerned with the pilot's perception of aircraft responsiveness. The expression for the CAP and its relation to pitch rate are given in Equations 6 and 7.

$$\text{CAP} = \frac{g\omega_{sp}^2 T_{\theta_2}}{V} \tag{6}$$

$$\frac{q(s)}{\delta_{CS1}(s)} = \frac{K_q\left(1 + T_{\theta_2} s\right)}{s^2 + 2\zeta_{sp}\omega_{sp} + \omega_{sp}^2} \tag{7}$$

The CAP can be defined as the ratio of the initial pitch acceleration response to the final steady-state normal acceleration due to an elevator or in the case of the Flying-V, elevon deflection. Based on Equation 6, CAP is closely related to the square of the short period frequency and the airspeed. From Tables 2 and 3, the short period frequency at the forward CG is 0.681 and 2.01, respectively, for the approach and cruise conditions. As a result, the CAP is expected to be smaller for approach. This indicates that the response of the aircraft along the pitch channel might feel more sluggish with decreasing speed. The CAP values and the handling qualities requirements are presented in Figure 6.

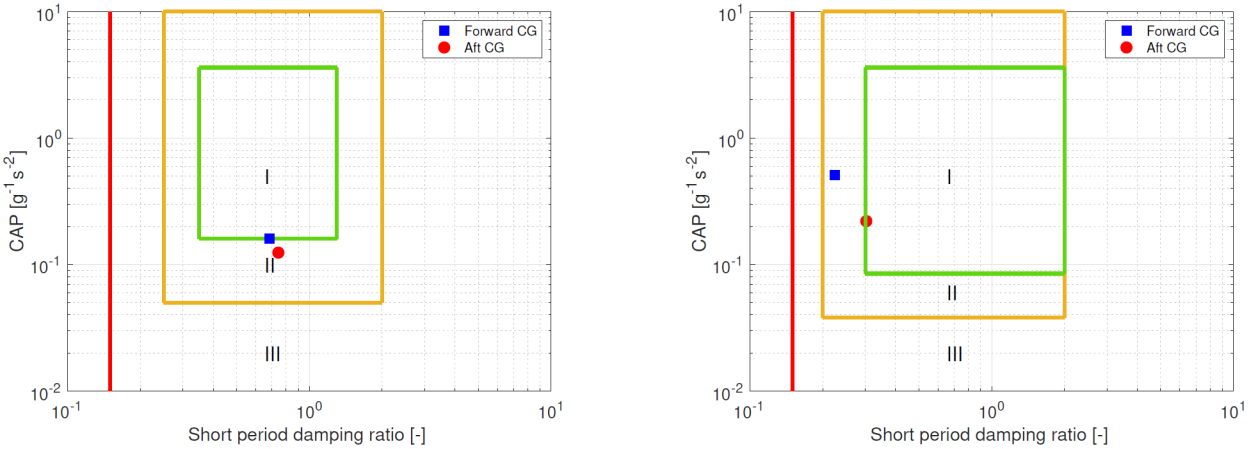

(a) CAP for approach phase.

(b) CAP for cruise phase.

Fig. 6 CAP values and requirements, taken from [10]

In this figure, the regions related to Levels 1, 2, and 3 are indicated by Roman numerals I, II, and III, respectively. Hence, it is straightforward to notice that during approach at the forward CG, the CAP is right between Level 1 and 2, whereas at the aft CG it is Level 2. For cruise at the aft CG, the CAP is between Level 1 and 2, while at the forward CG it exhibits level 2 handling qualities.

B. Augmented-airframe Analytical Handling Qualities

The FCS used for the augmented airframe is taken from Stougie [12]. In order to ensure that the FCS delivers desired performance, the control gains must be tuned properly. For this reason, a multi-objective optimization strategy is adopted, where the optimization constraints are set using performance requirements that are based on the MIL-STD-1797A [27] document. The optimization is divided into two separate tasks as the longitudinal and lateral tuning, and they are executed independently of each other. Separation of the tuning is viable since the scoring of each task is independent of the other. The tuning is only performed for the cruise condition at the forward CG location.

The longitudinal tuning uses handling quality requirements on the gain and phase margins of the pitch rate, short period frequency and damping ratio, CAP, bandwidth frequency, the equivalent time delay parameter, and the low-order equivalent system (LOES) fitting score. These constraints are used for minimizing the maximum control surface deflections, control surface activity, C* settling time, and C* overshoot. On the other hand, lateral tuning uses requirements on the gain and phase margin of roll and yaw rates, aperiodic roll and spiral time constants, Dutch roll frequency and damping ratio, and the LOES fitting score. Similarly, these are used to minimize control surface activity, maximum control surface deflections, and roll settling time. The results of the tuning procedure are given in Figure 5, where yellow cells indicate Level 2 handling qualities, and all the rest are Level 1.

Table 5 Tuning of the flight control system in cruise, obtained from [12]

(a) Longitudinal tuning results

Parameter	No Sensors	Adjusted Sensors	Baseline Sensors
GM on ν_q, dB	20.37	6.08	5.35
PM on ν_q, deg	65.34	48.06	34.5
ω_{sp}, deg/s	1.81	1.82	2.18
ζ_{sp}	1.29	1.12	0.79
CAP, $g^{-1}s^{-2}$	0.433	0.388	0.368
ω_{BW}, rad/s	3.27	3.17	3.12
τ_p, s	0.029	0.021	0.038
LOES$_{score}$	4.67	4.05	10.79

(b) Lateral tuning results

Parameter	No Sensors	Adjusted Sensors	Baseline Sensors
GM on ν_p, dB	24.28	7.91	6.97
PM on ν_p, deg	63.16	52.95	48.98
GM on ν_r, dB	26.29	7.19	5.85
PM on ν_r, deg	75.95	49.28	22.82
$1/T_s$, s^{-1}	0.074	0.065	0.07
T_r, s	0.513	0.604	0.52
ω_{dr}, rad/s	1.036	2.66	3.81
ζ_{dr}	0.26	0.52	0.74
$\omega_{dr}\zeta_{dr}$, rad/s	0.27	1.37	2.83
LOES$_{score}$	3.54	3.74	3.77

An important contribution of this tuning procedure is that this process was repeated for three different sensor configurations, which are no sensors, baseline sensors, and adjusted sensors. The tuning procedure without sensor dynamics yields Level 1 handling qualities for all parameters. However, when sensor dynamics are added for tuning, the gain and phase margins for the pitch and yaw rates decline to Level 2, while all the rest remain at Level 1. The main cause of this decline is the sampling rate and the time delay modeling of the angular rate sensor. Hence, to recover the handling qualities back to Level 1, an adjusted sensor model is proposed. The new model uses an angular rate sensor with a time delay of 0.04 seconds and a filter time constant of 0.03. The adjusted sensor model successfully recovers Level 1 handling qualities for all parameters. It is noted in [12] that as long as the sampling frequency of the angular rate sensor is equal to or above 100 Hz with a maximum time delay of 0.05 s, the FCS can be tuned to deliver Level 1 handling qualities.

In conclusion, the same FCS structure and final gains associated with the updated sensor model will be used for piloted evaluations. Hence, based on this offline analysis, the piloted evaluations of the augmented airframe should deliver level 1 handling qualities in cruise condition.

The next section will explain the experiment design for the simulator evaluations including the assessment methods, rating scales, maneuvers, tasks, flight conditions, the SIMONA Research Simulator, symbology for the tasks, pilot qualifications, and the experiment timeline.

V. Experiment Design

The experiment is designed with the objective of investigating the handling qualities of the bare and the augmented airframes. As explained in the previous sections, there are existing studies on the Flying-V using the same aerodynamic model and the FCS used in this paper. These studies make several claims regarding handling qualities based on offline simulations. Hence, one aspect of this paper is the validation of these claims through piloted tests. In addition to handling qualities, specific maneuvers are designed to test the flight envelope protection by pushing the aircraft towards the edges of the flight envelope.

A. Piloted Handling Quality Assessment Methods

There are several rating scales and requirements that allow quantifying the handling qualities of the aircraft during piloted simulations. For this paper, two primary rating scales and various requirements from the EASA CS-25 specifications are used. The first handling quality scale is the Cooper-Harper (CHRS) [20]. This scale helps the pilot rate aircraft behavior for a specific task to achieve desired performance. Fundamentally, the pilot will rate the adequacy of the aircraft for a pre-designated operation or mission. Hence, the validity of the CHRS is tied to the pre-defined desired and adequate metrics.

In addition to CHRS, a second rating scale is used to reveal the pilot-induced oscillation characteristics while performing tracking tasks. The AC 25-7D document from the U.S. Department of Transportation [21] outlines flight test procedures to demonstrate compliance with the CS-25 requirements. According to AC 25-7D, tracking and capture tasks can reveal PIO tendencies and assist in investigating pilot-aircraft couplings. Hence, including the PIO rating broadens the conclusions that can be drawn from piloted tests. The characteristic descriptions of PIO are available from the Federal Aviation Administration (FAA) and the military standard, MIL-STD-1797A [27]. However, for quantifying the results, military ratings will be used.

B. Experiment Tasks and Flight Conditions

This subsection covers all the tasks and maneuvers designed for the experiment. Overall, three types of maneuvers are considered, which are longitudinal, lateral-directional, and FEP. The definitions of each of these are explained in conjunction with their scoring and/or compliance requirements. The longitudinal and lateral-directional task and maneuver selections are derived from the AC 25-7D and CS-25 standards. The FEP maneuvers are designed based on the FCS design specifically for this study; hence, they do not come directly from any military standard or civil aviation authorities. For all tasks and maneuvers, the auto-throttle remains active to relieve the pilot from the responsibility of adjusting the thrust manually. Although none of the tasks require speed adjustment, in case the pilot deems it necessary to change the speed, they can do so by setting a new reference using the mode control panel. The longitudinal and lateral-directional tasks are performed for both the bare and augmented airframe in cruise, climb-out, and approach conditions. On the other hand, the FEP maneuvers are only performed for the augmented airframe in cruise condition. The definitions of the flight conditions are given in Table 6. During the longitudinal tasks, lateral sidestick and rudder pedal inputs are disabled to prevent accidental activation of the lateral-directional dynamics and to allow pilots to focus on the given task.

Table 6 Flight conditions for the maneuvers

Condition	TAS [Mach]	TAS [m/s]	Altitude [km]	Air Density [kg/m^3]
Approach	0.20	70	1	1.1116
Climb-Out at MTOW (Take-Off)	0.30	100	0.3	1.2250
Cruise	0.85	250	13	0.2655

1. Pitch Tracking (PT)

Pitch tracking is a task that looks at longitudinal motion and allows us to gain understanding of PIO susceptibility. For this task, a reference signal consisting of steps and ramps is generated. Starting from the trim condition, the pilot is asked to follow this pitch reference accurately enough to satisfy a pre-determined performance level, which is characterized by the adequate and desired performance scores that are displayed for the pilot during the experiment. The desired margin is defined as ±0.5 deg from the reference signal, whereas it is ±1 deg for the adequate margin. The calculated scores are based on the time the pilot is able to stay within the margins as a percentage of the time elapsed for the maneuver. Consequently, if the pilot is in the desired margins, both the desired and adequate scores will go up, whereas if the pilot is only in the adequate margins, the desired score will go down. The pilot is asked to attain 75% for desired compliance. Once the experiment is over, the pilot is asked to provide scores using the CH and PIO rating scales and to provide comments regarding aircraft behavior. An example pitch signal with associated margins is shown in Figure 7.

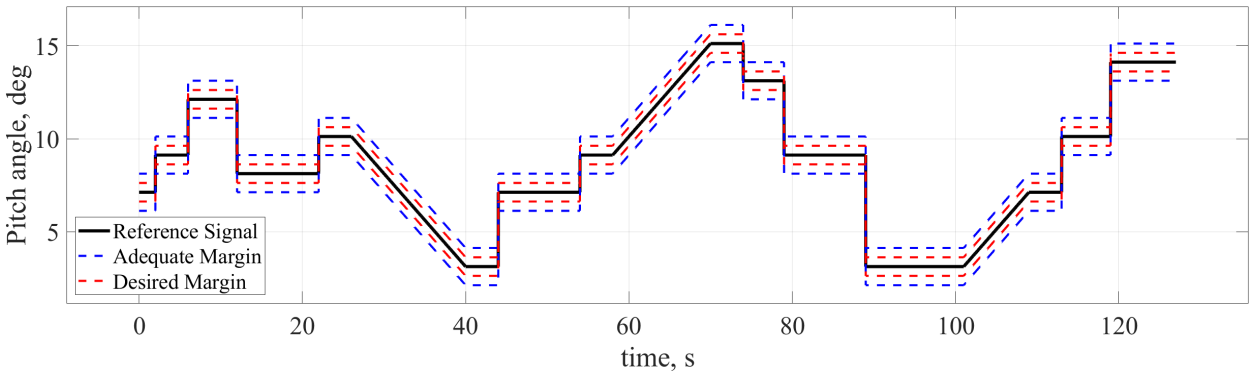

Fig. 7 Example pitch reference signal

2. Flight Path Angle Tracking (FPAT)

The second task focusing on longitudinal dynamics is the flight path angle tracking. This maneuver is a valuable addition to pitch tracking, as it is directly related to the aircraft's velocity vector. Looking into flight path angle provides insight into how well the aircraft's trajectory is controlled. The tracking is performed similarly to pitch tracking using a reference signal starting from the trim condition, where the desired and adequate margins remain the same. The reference signal used for FPAT is less aggressive than the pitch tracking. This is because the flight path angle dynamics are slower than the pitch dynamics. The pilot is asked to obtain a score of 75% for desired compliance. A flight path marker and scores are available to the pilot during the task. Once the experiment is over, the pilot is asked to provide scores using the CH and PIO rating scales and to provide comments regarding aircraft behavior.

3. Pitch Capture (PC)

The last maneuver for longitudinal dynamics is the pitch capture. This task is based on Section 5.1.4.4 of AC 25-7D [21]. The pilot is asked to capture a sequence of pitch angles changing in 5 or 10 degree increments. There is no scoring in this section, as pilots are asked to capture the pitch at their own pace, allowing them to freely comment on the aircraft behavior without worrying about the desired performance.

4. Coordinated Turn (CT)

A particularly interesting maneuver that focuses mainly on lateral-directional motion is the coordinated turn. This maneuver aims to test the aircraft's capability to coordinate yaw, pitch, and roll together. To this end, the pilot is asked to turn at a constant speed while minimizing the sideslip angle, which is available on the head-up display during the maneuver. According to CS 25.143 (h), a bank angle between 40 and 45 degrees and a flight path angle between 0 and 5 degrees are required for compliance. The maneuver will be considered satisfactory if the pilot can keep the aircraft within the target margins for 10 seconds.

5. Bank-to-Bank (BTB)

According to AMC 25.147(f) [22], an aircraft must be able to go from a 30 degrees steady banked turn to 30 degrees opposite bank in 7 seconds for lateral control compliance. For this, starting from trim, the pilot is asked to reach a bank angle between 30 and 36 degrees, while keeping a flight path angle between 0 and 5 degrees. Once the pilot leaves the first target with all margins satisfied, a timer is displayed for the pilot, and simultaneously a marker indicates the next bank angle target in the opposite direction. The maneuver is considered satisfactory once the pilot successfully reaches the opposite bank under 7 seconds.

6. Steady Heading Sideslip (SHS)

Steady Heading Sideslip (SHSS) is a maneuver that allows assessing the crosswind capabilities of an aircraft. The goal is to keep constant heading while the aircraft has non-zero sideslip. AMC 25.177(c) provides a formula to determine the appropriate sideslip angle as a function of airspeed for this maneuver: $\beta_{req} = \arcsin(30/V)$ where V is calibrated airspeed in knots. This leads to a sideslip requirement of 13.4, 9, and 7.4 degrees for approach, climb-out, and

cruise, respectively. These are rounded off to 15, 10, and 5 degrees to make the task slightly more difficult in cruise and easier in approach. Starting from the trim condition, the pilot is asked to capture the indicated sideslip while holding the flight path angle between 0 and 5 degrees. The maneuver is considered complete if the pilot can maintain a constant heading within a margin of ±7.5 degrees for 10 seconds while keeping constant speed.

7. Dutch Roll (DR)

As a part of its unique design, the Flying-V lacks a fuselage and a vertical tail. A consequence of this is that the aircraft body has a harder time damping any undesired lateral-directional oscillations. For the bare-airframe model, as seen in previous sections, the Dutch roll is known to be unstable. However, the FCS used for this experiment promises level 1 handling qualities in cruise condition, including the Dutch roll. Hence, it is valuable to demonstrate how well the FCS is able to compensate for the Dutch roll, its effect on pilot experience, and the degree of Dutch roll instability in the bare-airframe model. To this end, starting from a steady trim condition, the pilot is asked to excite the Dutch roll through a sideslip/rudder doublet input, and once the aircraft is in a sustained oscillation, to counteract this using any means available.

8. Free Roll Captures (FRC)

For this maneuver, the pilot has complete freedom to capture bank angles in increments of 5 to 10 degrees. The goal of this is to allow pilots to comment on the aircraft behavior while they resort to their natural flying instincts without worrying about the margins and the desired performance.

9. High-Bank Descending Turn (HBDT)

This maneuver aims to test the roll protection feature of the FCS. For this, starting from trim, the pilot is asked to apply a continuous lateral stick input while slowly descending. Roll protection becomes active once the bank angle reaches 66 degrees. During the maneuver, the flight path angle must be kept between 0 and -20 degrees. The goal of the descent is to prevent the aircraft from reaching a load factor of 2.5. If that were to happen, the load factor protection would become active and would push the aircraft's nose down, interfering with roll testing. The maneuver is considered satisfactory if the pilot can descend while keeping a bank of 66 degrees for 10 seconds, and afterward is able to recover to a zero bank and a flight path angle between -5 and 5 degrees.

10. Full-Pitch Ascending Turn (AT)

This maneuver focuses on testing the load factor protection of the FCS. The pilot is asked to reach a bank angle of 45 degrees while maintaining a positive flight path angle. Once the initial target is satisfied, the pilot should apply maximum pitch deflection with the sidestick and hold it for 20 seconds. This will push the load factor to 2.5 and activate the protection system. Once the pilot is able to hold everything inside the margins for 20 seconds, is asked to recover to zero bank and a flight path angle between -5 and 5 degrees for a successful maneuver.

C. Experiment Simulator

The experiment is carried out in the SIMONA Research Simulator (SRS) [19] of the Delft University of Technology. SRS is a 6-DOF, motion-based simulator that possesses a flight deck, a visual display system, and a control loading system. During the experiment, the motion system of the SRS remains inactive. This is due to the high-g nature of the maneuvers for the FEP testing, and for the rest of the maneuvers, the contribution of the motion system is assumed to be minimal on the pilot's flight experience. Figure 8 shows the SRS from the outside and its interior.

An essential part of the simulator is the head-up display (HUD), which can be seen in Figure 8b located in the middle. The flight parameters that are most relevant for the operation are communicated to the pilots through the HUD. The display has a default layout to show these parameters, and there are additional layouts for each task. The default layout is given in Figure 9.

In this default HUD configuration, "A" is the load factor, "B" is indicated airspeed in kts, "C" is the Mach number, "D" is the thrust level as a percentage of the maximum thrust, where the yellow line is the thrust needed for trim, "E" is the pitch ladder, "F" is the pitch indicator, "G" is the flight path angle marker, "H" is the altitude in feet, and "I" provides the AoA, sideslip angle and flight path angle in degrees.

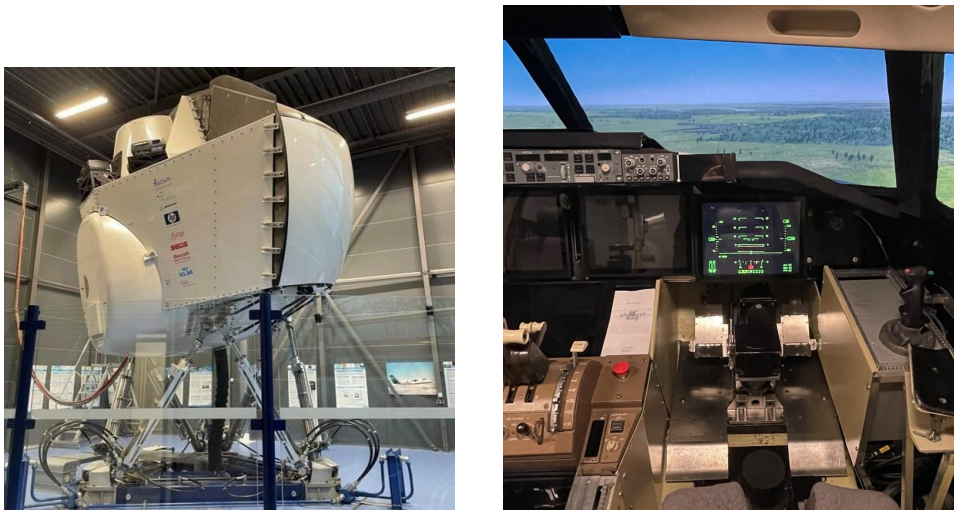

(a) SRS from the outside

(b) SRS from the inside

Fig. 8 SIMONA Research Simulator

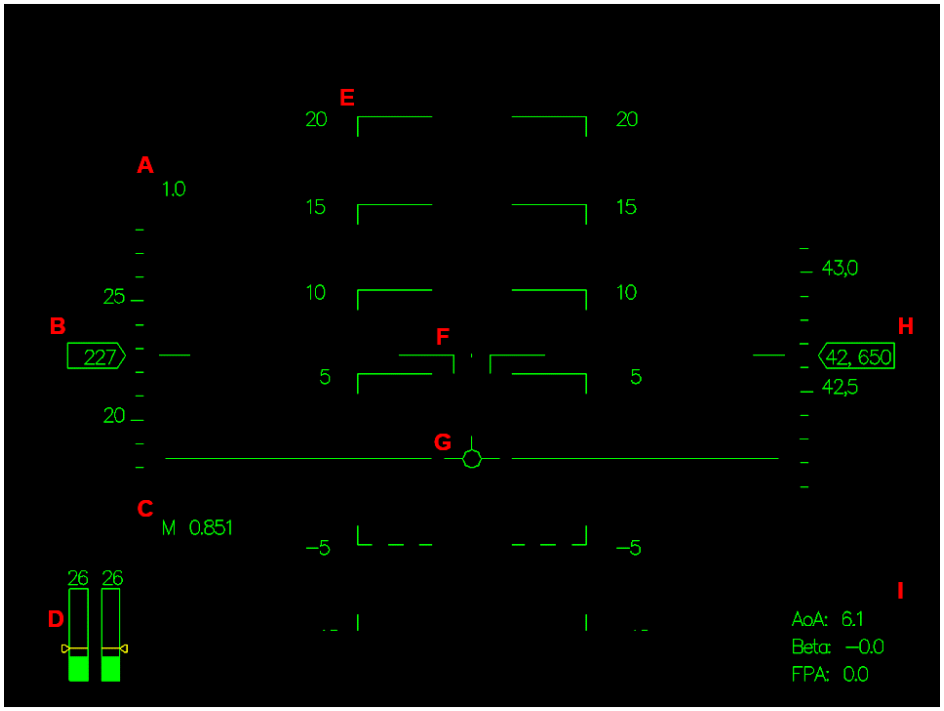

Fig. 9 Default HUD configuration

D. Experiment Participants and Structure

The experiment is conducted with three different pilots. Two of the pilots are technical test pilots for commercial aircraft, whereas the third pilot is both a flight test engineer and a US National Test Pilot School alum. The pilots and their credentials are given in Table 7.

The simulation is performed in blocks for all pilots. The experimental sections are grouped into longitudinal, lateral-directional, and FEP maneuvers for bare and augmented airframes. A total of five simulation blocks are designed. The overall progression of each experiment session is given in Table 8.

Pilots A and C had complete availability to go through the simulation blocks in this order; however, Pilot B had

Table 7 Pilots and their credentials

Pilot	Credentials
A	Technical Pilot (commercial aircraft)
B	Flight Test Engineer, US National Test Pilot School Alum
C	Technical Pilot (commercial aircraft)

Table 8 Simulation blocks

Simulation Blocks	Tasks
1. Longitudinal (Bare-Airframe)	Pitch Tracking Flight Path Angle Tracking Pitch Capture
2. Longitudinal (Augmented-Airframe)	Pitch Tracking Flight Path Angle Tracking Pitch Capture
3. Lateral-Directional (Bare-Airframe)	Dutch Roll Coordinated Turn Bank-to-Bank Steady Heading Sideslip Free Roll Captures
4. Lateral-Directional (Augmented-Airframe)	Dutch Roll Coordinated Turn Bank-to-Bank Steady Heading Sideslip Free Roll Captures
5. FEP (Augmented-Airframe)	High-Bank Descending Turn Full-Pitch Ascending Turn

limited availability. As a result, for that session, the longitudinal tasks for the bare and augmented airframes were grouped in a single block, and the FPAT task was removed. In the second block, lateral-directional maneuvers for the augmented airframe were considered together with the FEP tasks, and lastly only the Dutch roll was considered for the bare-airframe lateral-directional block.

The next section will outline the results of these experiments, including the ratings, pilot comments, and data analysis based on the experiment logs as well as pilot inputs, and will provide a discussion of the findings. In addition, a comparative conclusion will be presented between the theoretical handling quality expectations based on offline analysis and the experiment results.

VI. Results and Discussion

This section aims to present the results and provide a well-reasoned discussion using the data collected during the experiment. The results are grouped into three categories, longitudinal, lateral-directional, and FEP. Each category provides ratings, pilot comments, and where necessary, an analysis of the experiment data logs.

A. Longitudinal Results

The longitudinal tasks are the pitch tracking (PT), flight path angle tracking (FPAT), and pitch capture (PC). PT and FPAT use scoring systems in relation to desired and adequate performance levels. Setting these levels is an essential part of the evaluation, as they indicate the validity of the Cooper-Harper ratings given by the pilots. As explained in the

previous section, the desired score for PT and FPAT is set to be 75%. The calculation of the score is based on how long the pilot is able to stay inside the margins as a function of the total time elapsed for the task. So, before moving on with the CHRS and PIO results, it makes sense to look at the desired and adequate scores the pilots are able to achieve. These scores are given in Figure 10 for all longitudinal tasks performed during the experiment. It is important to reiterate that the lateral sidestick and rudder pedal inputs are disabled for these maneuvers; therefore, the pilots did not use roll or yaw inputs to perform the task. Also, due to limited availability of Pilot B, the FPAT task is removed from that session.

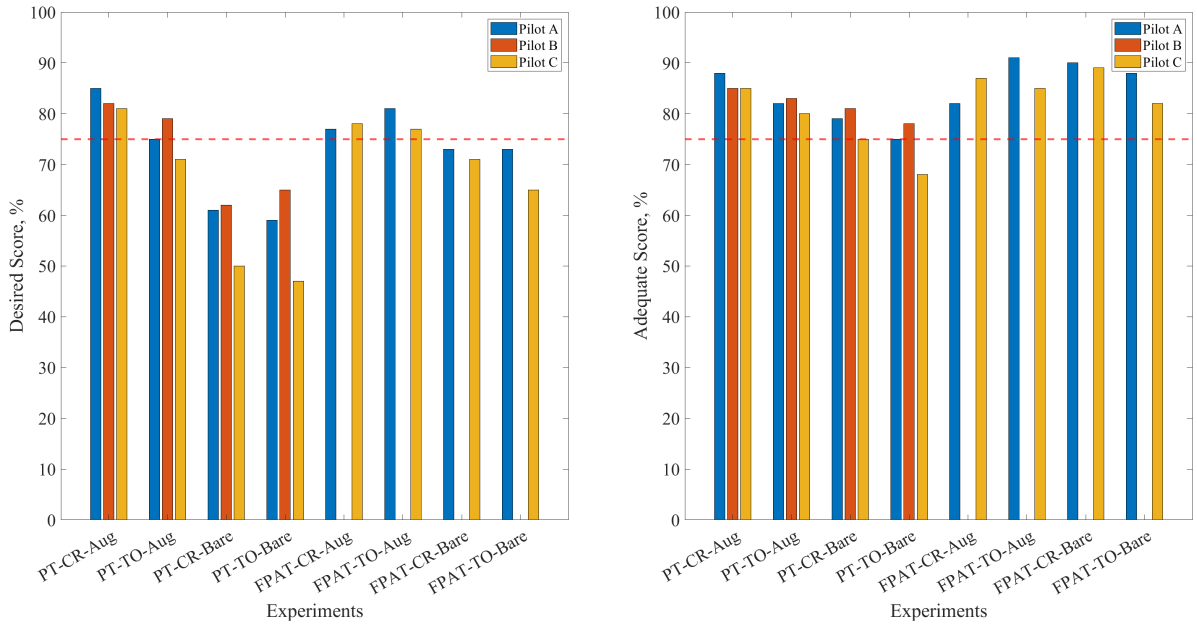

(a) Desired scores **(b) Adequate scores**

Fig. 10 Desired and adequate scores for all longitudinal tasks

Before analyzing the figure, it is important to mention that almost all pilots commented that longitudinal tasks were highly demanding for a commercial airliner. Consequently, the requested performance limit was also deemed high. This means that adjusting the difficulty of the tasks to be more operationally relevant with proper scoring targets can lead to higher scores and a lower performance threshold.

The abbreviations CR and TO stand for cruise and take-off, respectively. By direct inspection of the figures, it is possible to notice several trends. First, especially for the pitch tracking task, switching from augmented to bare airframe leads to a significant reduction of the desired score. This is an expected observation and a positive indication that the FCS is able to provide substantial performance improvements. The score reduction between the bare and augmented airframe is less pronounced in the flight path angle tracking task. This disparity in the tracking results can be explained by the additional dynamics between the pitch and flight path angle. Since the dynamics considered for this section are purely longitudinal, the flight path angle can be defined as the difference between pitch and angle of attack. The pitch angle describes the aircraft's orientation with respect to the horizon, whereas the flight path angle defines the aircraft's velocity vector. Hence, considering that the speed is constant during the experiment due to auto-thrust, changing the flight path angle first requires a change in pitch. The response of the flight path angle to these changes is, by nature, slower and more damped. Consequently, it is easier for pilots to stay within the margins for the FPAT task. Additionally, the scores for the cruise condition tend to be higher compared to take-off. This is because the aircraft is considerably faster in cruise condition, where the control effectiveness is higher.

Now that the scores are established, it is interesting to visualize how these translate into actual Cooper-Harper and PIO scores. Figure 11 gives the ratings for all longitudinal tasks and the associated handling quality classifications. Fundamentally, the Cooper-Harper rating scale is a qualitative measure that depends on some desired performance criteria and the pilot's judgement on the aircraft behavior for a specific task. On the other hand, PIO rating is reflective of pilot-aircraft couplings. As a result, it is difficult to find a direct correlation between these ratings and the handling quality levels defined in the military standard MIL-F-8785C [26]. Fortunately, another military standard, MIL-STD-1797A [27], provides handling quality categories for the PIO and CH rating levels.

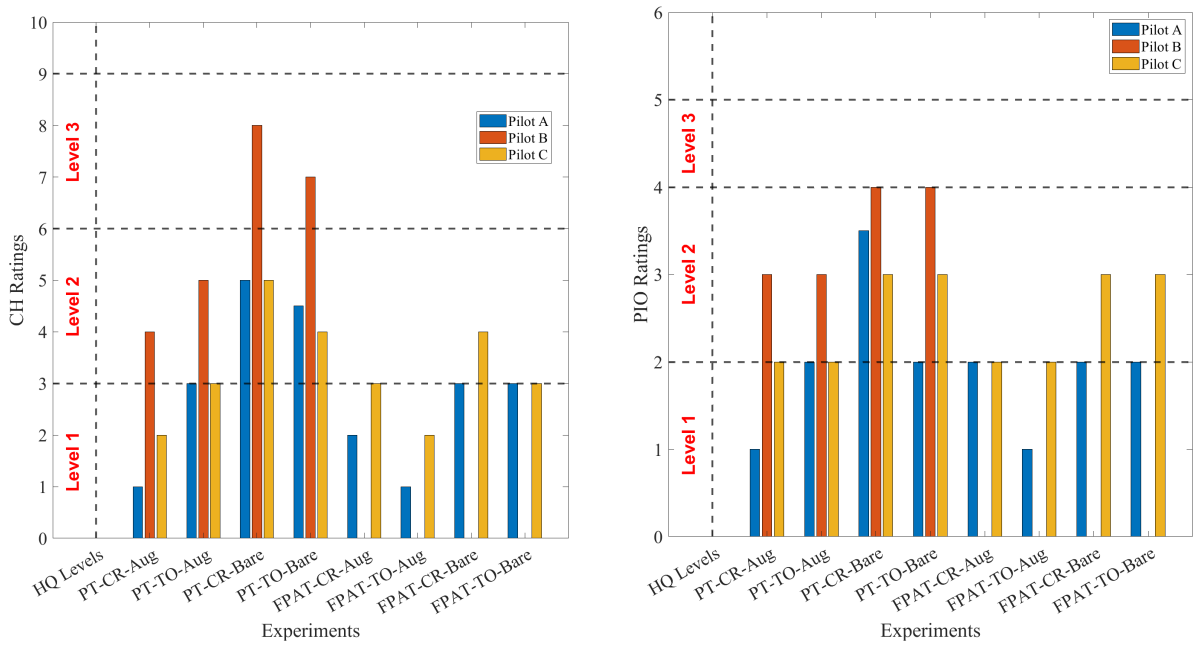

(a) Cooper-Harper Scores **(b) PIO Scores**

Fig. 11 Cooper-Harper and PIO ratings for all longitudinal tasks

Judging from the figures, for both ratings, the augmented airframe results are all within Level 1 according to Pilots A and C. On the other hand, Pilot B, who could only perform the pitch tracking task, deemed the handling quality to be Level 2. For the bare-airframe, pitch tracking scores of Pilot A and C moved towards Level 2. However, Pilot B gave a CH rating of Level 3 and a PIO rating of Level 2. The score disparity between pitch tracking and flight path angle tracking seen in Figure 10, exhibited itself in the ratings as well. Almost all FPAT tracking tasks are in the Level 1 range, with only some Level 2 ratings for the bare-airframe in cruise and take-off conditions.

During the experiments, pilots are asked to comment on the behavior of the aircraft while performing the tasks and to provide an explanation for their ratings. In general, pilots commented that longitudinal tasks with the augmented airframe are well-controllable, predictable, and realistic. For pitch and flight path angle tracking, reference signals are regarded as difficult to follow when the load factor buffet limit is kept between 0.7 and 1.3. However, they are deemed followable if the load factor buffet limit is increased to be between 0.4 and 1.6, which is significantly greater than conventional aircraft configurations. Also, the auto-thrust is mentioned to work nicely. Conversely, some comments note slight over and undershooting tendencies from the pilots in case of aggressive inputs. The pitch response is found to exhibit small oscillations, together with slight dropback behavior and sluggishness, which nicely corresponds to the CAP expectations outlined in Section IV.A.2. One pilot mentions that lowering the input aggressiveness solves the dropback, oscillations, and under/overshooting tendencies but makes it difficult to attain desired performance. Figures 12 and 13 show the load factors and pitch behavior of Pilot A using low and high aggressiveness during pitch tracking. Following the signal more aggressively violates the load factor buffet limits, but makes it easier to achieve the desired score.

Expectedly, the pilots had a more difficult time with the bare-airframe model for the same tasks. The aircraft was commented to be stable and controllable, but only with significant pilot effort. Compared to the augmented airframe, the pitch rate damping was mentioned to be much worse, and the PIO tendencies were more significant. In addition, the stick deflections were more sensitive, which led to a higher workload for the pilots. This could be due to the linear nature of the mapping between the sidestick and control surface deflections, which does not take flight condition into consideration. Interestingly, for the tasks in take-off condition, one pilot commented that the aircraft feels unstable with high-frequency but small-amplitude oscillations. However, another pilot mentioned better pitch rate damping and lower PIO tendencies for the same task. Furthermore, the pitch response was found to be more sensitive in take-off compared to cruise.

Lastly, none of the tasks could be performed in approach condition due to very low control authority, and high angle of attack values necessary to trim the aircraft. Trimming the aircraft in approach requires around 23 degrees AoA, and

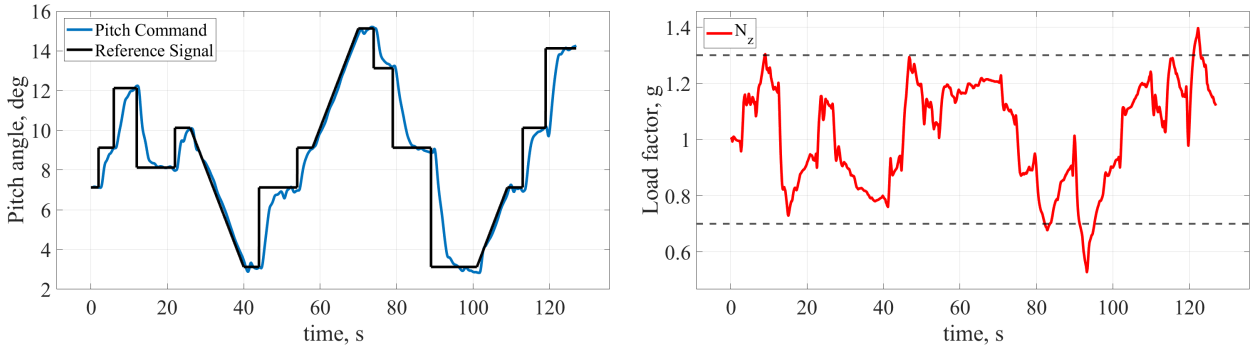

Fig. 12 Pitch and load factor behavior for low aggressiveness

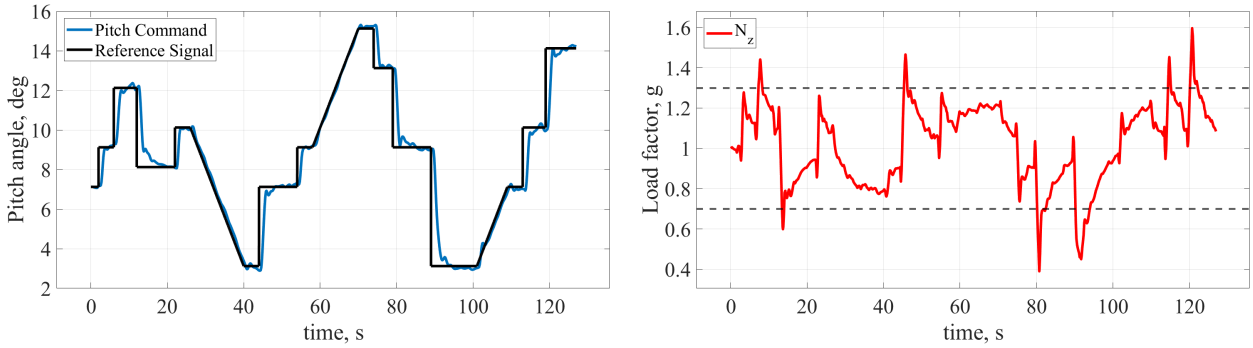

Fig. 13 Pitch and load factor behavior for high aggressiveness

around 20 degrees deflection for all elevons. This AoA value immediately activates the AoA protection system for the augmented airframe, and since the control deflection limit is set to 25 degrees for the elevons due to actuator limitations, the remaining control authority is not sufficient to track any reference signal.

B. Lateral-Directional Results

The lateral-directional tasks are the Dutch roll, coordinated turn, bank-to-bank, steady heading sideslip, and free roll captures. In contrast to longitudinal tasks, these maneuvers are not assessed through a scoring and/or rating system. As mentioned previously, these maneuvers are designed specifically to demonstrate compliance with the EASA CS-25 rules and are evaluated on a pass/fail basis. For free roll captures, no evaluation criteria are used, and the only outcome collected is verbal pilot feedback. Table 9 shows the results for all maneuvers, where (!) indicates a conditional pass as explained in more detail in the following sections.

The criteria for passing and failing each task are described in Section V. Moreover, due to the limited availability of Pilot B, only two cases could be tested for the bare-airframe. Nevertheless, as it will become clear during the discussion, this does not change the validity of these results. The discussion is divided into two as augmented and bare-airframe.

1. Augmented Airframe

From the table, almost all maneuvers were successful for the augmented airframe except for the steady heading sideslip in take-off condition. For this maneuver, obtaining a sideslip angle of 10 degrees is required while keeping the heading constant. The failure is caused by the aircraft's inability to follow the sideslip command given by the pilot through the pedals. The pilots indicated the possibility of rudder saturation. Therefore, an investigation of the experiment data logs revealed that the rudders are in fact saturating before the commanded sideslip can be attained. Figure 14 shows the commanded and measured sideslip angles, as well as the control surface deflections for the SHS maneuver performed by Pilot C in take-off condition. As seen in the figure, initially the actual sideslip is able to follow the command; however, at around 20 seconds, the rudder starts saturating and the sideslip can no longer follow the commanded value.

Table 9 Results for all lateral-directional maneuvers

	Augmented-Airframe			Bare-Airframe		
Maneuvers	Pilot A	Pilot B	Pilot C	Pilot A	Pilot B	Pilot C
DR-CR	Pass	Pass	Pass	Pass	Pass	Fail
DR-TO	Pass	Pass	Pass	Pass	-	Fail
CTC-CR	Pass	Pass	Pass	Fail	Fail	Fail
CTC-TO	Pass	Pass	Pass	Fail	-	Fail
BTB-CR	Pass	Pass	Pass	Pass(!)	-	Pass(!)
BTB-TO	Pass	Pass	Pass	Pass(!)	-	Pass(!)
SHS-CR	Pass	Pass	Pass	Fail	-	Fail
SHS-TO	Fail	Fail	Fail	Fail	-	Fail

The pilots successfully completed the remaining maneuvers while providing feedback for each of them. They characterized the Dutch roll as perfectly stable, 'deadbeat', and self-damping without requiring pilot input. One pilot even commented that the Dutch roll behavior of the augmented airframe is better than a commercial airliner with which they have experience.

For coordinated turn, pilots noted the desirable characteristics of the augmented aircraft and good turn coordination during cruise conditions. However, they commented on the high back pressure relative to roll input during turns, revealing a discrepancy in sensitivity between pitch and roll channels. One pilot also observed a slight lag in turn coordinated in take-off conditions.

The bank-to-bank maneuver in cruise condition is considered to be stable, as all pilots are able to perform the task with dynamic and stable captures. Nevertheless, in take-off condition, pilots mentioned a slight PIO tendency, roll hesitation, and pitch dropout, especially when high roll inputs are applied. The pilot who experienced the pitch dropout suggested that it might be due to elevon saturation. Investigating the data after the experiment confirmed the suggestions of the pilot. Figure 15 shows the inputs given by the pilot during the BTB maneuver and the control surface deflections. This figure does not include the rudder deflections, as it would further complicate the plot and does not add value for this specific analysis. From the inset of these figures, it can be seen that around 13 seconds from the beginning of the experiment, the elevons start to saturate. The effect of saturation is clear from the pitch angle plot, where the saturation of CS1R and CS2L leads to a slight initial increase, as the remaining control surfaces try to compensate for the saturation. This is followed by a sudden pitch drop once the remaining surfaces saturate as well. The saturation limits of the elevons are indicated by black dashed lines.

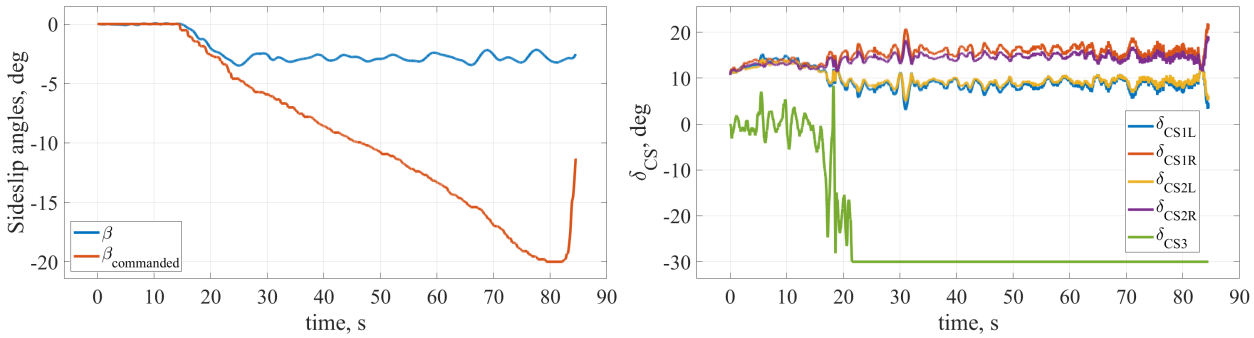

Fig. 14 Sideslip angles and control surface deflections: augmented airframe, SHS maneuver, TO condition

Lastly, during the free roll captures, pilots commented good turn coordination and easy bank control. On the other hand, they reported small pitch and sideslip oscillations while capturing various roll targets. Similarly to the bank-to-bank discussion, one pilot commented that large roll inputs drop the nose slightly, which, as already explained, is due to elevon saturation.

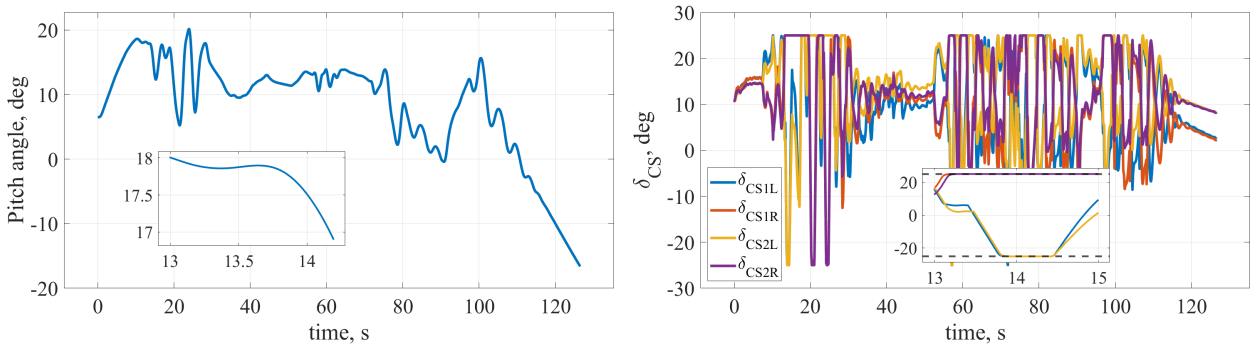

Fig. 15 Pitch angle and control surface deflections: augmented airframe, BTB maneuver, TO condition

2. Bare-Airframe

From Table 9, it is clear that the bare-airframe model performs significantly worse than the augmented airframe, as almost all maneuvers fail. The core reason for these failures is the very poorly damped Dutch roll. In the section related to handling quality expectations, the Dutch roll is stated to be unstable for the bare-airframe model at the forward CG location. Hence, this result is not surprising; however, the extent of instability is worse compared to the previous lateral-directional piloted study on the Flying-V [7]. The degradation of lateral-directional behavior could be explained by differences in the aerodynamic model between the two studies.

The pilots found the Dutch roll to be quite challenging and difficult to control. Most of the remarks by the pilots had similar themes. They mentioned that the Dutch roll by itself does not dampen out without pilot intervention, and there is a lot of adverse yaw present. The recovery method was found to be highly unusual in the sense that conventional recovery techniques lead to divergent behavior. It was noted that rudder-only recovery strategies make the situation worse. However, the oscillations were less pronounced when unloading, and for singlet inputs. Applying small sideslip corrections while unloading was proposed as a potential effective recovery technique. In addition, pilots commented that being able to see the horizon and activating the motion system of the simulator could help with recovery.

All remaining maneuvers suffer from the Dutch roll instability. The only maneuver that could be satisfied was bank-to-bank. However, as can be seen in Table 9, the result of the BTB maneuvers has "(!)" right next to them. This mark indicates that the requirements for those maneuvers could only be satisfied through dynamic captures. Compliance with bank-to-bank does not specify any stability or overshoot limitations and solely focuses on the aircraft's ability to change a 60-degree bank under 7 seconds. As a result, the pilots were able to capture the target dynamically without caring for yaw stability or roll overshoot. All attempts made by the pilots in a slow and steady way ended up exciting the Dutch roll, leading to failure.

Coordinated turn results draw a similar picture to that of bank-to-bank. Accomplishing the maneuver becomes an impossible task once the Dutch roll is excited. Pilots commented that even small roll inputs are sufficient to start the Dutch roll. Figure 16 shows the control surface deflections, sideslip angle, and the aircraft Euler angles for a CTC experiment run.

Due to the implementation of open-loop or bare-airframe control allocation, matching elevons on the right and left sides are always deflected with the same angle. As a result, they cannot be used to generate any yawing moment. As explained during the experiment design section, the goal of the CTC maneuver is to capture a bank angle between 40 and 45 degrees and hold for 10 seconds while keeping the sideslip as close to zero as possible. So, if there is no coupling between roll and yaw, no rudder input should be necessary to perform the task, since the elevons are not capable of generating sideslip. However, in Figure 16, it can be seen that even though the pilot did not use any rudder input, the sideslip angle started to oscillate in a divergent manner. As the sideslip oscillations progress, the roll angle also starts to develop divergent oscillations. Expectedly, the steady heading sideslip shows the exact same behavior. None of the pilots could achieve the task in any flight condition due to Dutch roll excitation.

Finally, for free roll captures, pilots found the yaw damping to be lacking, and noted that the large elevon deflections lead to oscillatory behavior. It was also commented similar to the CTC that even small bank angles trigger the Dutch roll.

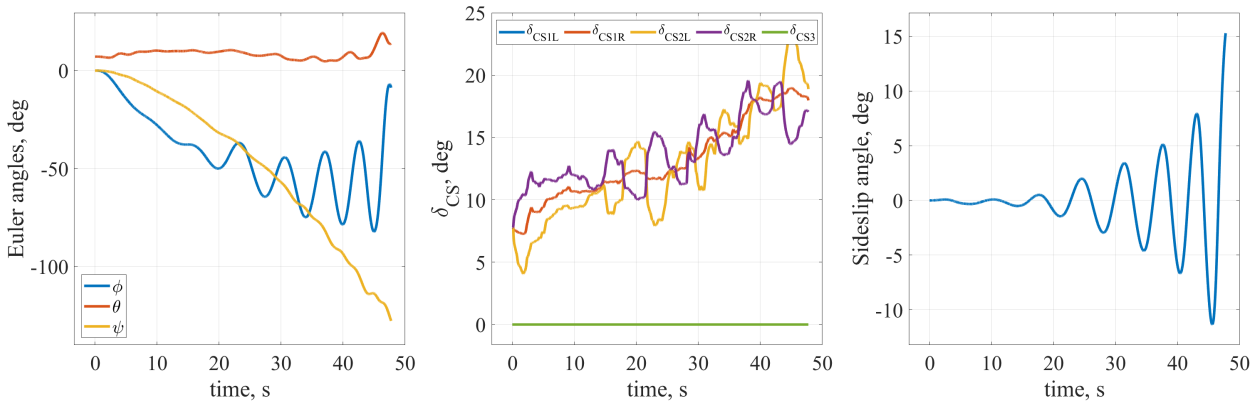

Fig. 16 Control deflections, Euler and sideslip angles: bare-airframe, CTC maneuver, CR condition

C. FEP-FCS Results

The maneuvers to test the flight envelope protection system are designed specifically for this experiment based on the characteristics of the flight control system. Hence, they are not directly available from military standards or civil aviation rules. The pilots did not comment that these maneuvers were unrealistic and seemed to understand the nature and purpose of them effortlessly.

The high-bank descending turn maneuver (HBDT) is designed to test roll protection without activating load factor protection. The pilots noted that if the rate of descent is not sufficient, the load factor protection becomes active, which interferes with the roll limit testing. So, during the experiment, the simulation had to be repeated 3 or 4 times until the pilots had some training and were able to adjust their descent rate. Figure 17 shows the results of the HBDT maneuver. The results reveal a considerable overshoot over the bank angle limit. Although the load factor remains below 2.5 to prevent interference with the roll protection task, the roll angle overshoots approximately 10% above the limit. This roll limit of 66 degrees is already quite larger than conventional airliners. However, the results are still relevant since the overshoot is not related to the roll limit but rather to the dynamics of roll protection. Furthermore, the second part of the task, which is recovery, could not be performed successfully by the pilots due to departure tendencies. Toward the end of the maneuver during recovery, the load factor starts oscillating and jumps out of its boundaries in a divergent way. This was an interesting finding, because departure tendencies were not stated nor identified during the offline analysis, which underlines the importance of pilot-in-the-loop simulations.

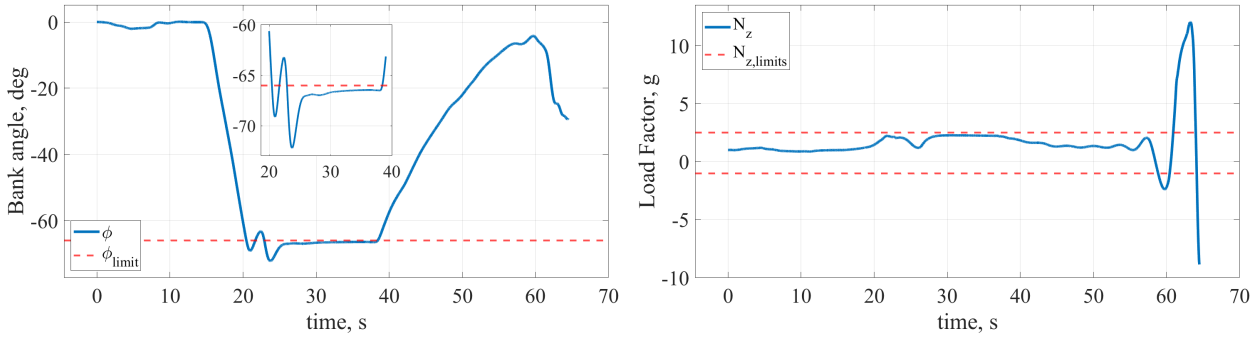

Fig. 17 Load factor and bank angle: augmented-airframe, HBDT maneuver, CR condition

The second and last FEP maneuver is the full-pitch ascending turn. In contrast to the previous one, the goal of this maneuver is to assess the load factor protection. To this end, pilots are asked to capture a bank angle and give full pitch deflection to push the load factor to its limits and hold for 20 seconds. Similarly to roll protection, the load factor is also prone to overshoot. The pilots noted some pitch and roll oscillations due to the load factor protection. However, recovery is successful and steady for all pilots. Figure 18 compares the actual and commanded load factors during this maneuver and shows the pitch and roll angles.

From the figure, it is clear that for the maximum load factor command of 3, the actual load factor fails to stay within

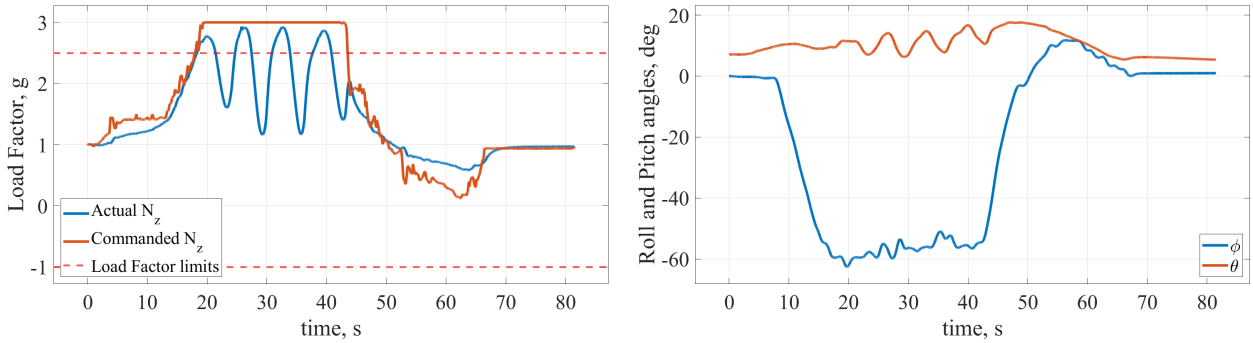

Fig. 18 Commanded and actual load factors, roll and pitch angles: augmented-airframe, AT maneuver, CR condition

its boundaries and oscillates in and out. However, other than the oscillation, the load factor protection gives a good performance in its ability to bring the load factor below the limit. Also, it is possible to comment that even though they exist, the pitch and roll oscillations are not divergent.

VII. Conclusions

This study focused on conducting piloted simulator experiments to validate recent claims regarding the handling qualities of the Flying-V simulation model and the flight control system. These claims come from offline studies that involve the development of an aerodynamic model and the design of the flight control system. The simulator experiments are performed for both the bare-airframe model that does not include a flight controller in the loop, and the augmented-airframe that uses an Incremental Nonlinear Dynamic Inversion (INDI) based flight control system with C*, roll rate, and sideslip controllers in the outer loop. The flight control system also includes a flight envelope protection system for bank, angle of attack, and load factor protection.

To assess handling qualities, several longitudinal and lateral-directional maneuvers were designed to demonstrate compliance with the EASA CS-25 rules and establish qualitative handling quality levels using Cooper-Harper and PIO rating scales. In addition, some aggressive maneuvers were formulated to test the flight envelope protection capabilities of the FCS to expose potential issues. A total of three pilots were invited to join the experiment and perform these maneuvers in the SIMONA Research Simulator of Delft University of Technology. During the experiment, pilots provided verbal feedback on aircraft performance and used the rating scales in relation to desired performance characteristics.

Judging strictly from the longitudinal results for the bare-airframe, most longitudinal results were between level 1 and level 2, showing a behavior similar to offline expectations. Regarding lateral-directional compliance, almost all maneuvers failed due to Dutch roll instability. This was also expected since the Dutch roll at the forward center-of-gravity was noted to be unstable in a previous study. On the other hand, for the augmented airframe, the results mostly fell in the level 1 category, which similarly is in alignment with the non-piloted results. The pilots were pleasantly surprised with the flight control system's ability to dampen out the Dutch roll. The FCS managed to turn this unstable and divergent mode into a characteristic that is perfectly stable and easy to manage. In addition, except for the SHS maneuver, which failed due to insufficient lateral-directional control authority, all other maneuvers could be performed to show compliance with the requirements. However, pilots noted slight pitch dropouts and oscillations, especially for large roll inputs, caused by elevon saturation.

It should be noted that it is not trivial to draw conclusions based on the results of the simulator test campaign. Although there seems to be a strong correlation between the piloted and offline results, the validity of the aerodynamic model to represent the Flying-V remains a significant question that brings a level of ambiguity to both the offline and piloted results. Another concern is the implementation of the flight control system. The control system used in the simulator was accepted as a correct and accurate implementation. However, since there are many elements to the controller that can have an impact on the handling qualities, it is not possible to be exactly sure about the viability of the implementation. Lastly, there is a slight mismatch between the real-time simulation platform and the offline Simulink environment caused by the adjustments that were necessary to generate C codes from the Simulink model. Hence, all of these factors must be taken into consideration when making a judgement on this version of the Flying-V simulation

model and for proposing new research directions.

In light of this, two categories of directions are considered for future research. The first is to address the concerns and ambiguities explained in the previous paragraph by validating that the simulator, model, and control implementations are correct. The second direction is to address poorly damped structural couplings and insufficiencies in control authority. The second research direction requires further research on structural and aerodynamic modeling, simulation, engine placement, landing gears, and the identification of the Flying-V model. In fact, there are a few recent studies that aim to tackle these problems [28–30]. These involve using handling quality criteria with offline simulations to size the control surfaces, concept design of a new subscale research demonstrator, and the design of a new aerodynamic model for the full-scale Flying-V model.

In terms of flight control, even though the tested FCS is capable of stabilizing the aircraft, the flight envelope protection cannot keep the bank, AoA, and load factor strictly within the limits. Hence, the implementation of the FEP should be re-evaluated. Also, the auto-thrust functionality of the flight controller is overly aggressive; so, the engine dynamics and the associated gains should be re-designed to make the changes in thrust more gradual. Finally, this experiment could study only one center-of-gravity location and two flight conditions. In the future, a wider range of CG locations and flight conditions should be investigated in piloted experiments.

Acknowledgments

This publication is part of the project Flying V Flight Control with project number 19511 of the Open Technology Programme, which is (partly) financed by the Dutch Research Council (NWO). The authors would like to acknowledge the in-kind contributions to the project of KLM Royal Dutch Airlines and ADSE. In addition, the authors thank all pilots who participated in the experiment for their time and valuable insights.

References

[1] Martinez-Val, R., "Flying Wings. A New Paradigm for Civil Aviation?" *Acta Polytechnica*, Vol. 47, No. 1, 2007. https://doi.org/10.14311/914.

[2] Benad, J., "The Flying V - A new Aircraft Configuration for Commercial Passenger Transport," *Deutscher Luft- und Raumfahrtkongress*, Deutsche Gesellschaft für Luft- und Raumfahrt - Lilienthal-Oberth e.V., Bonn, 2015. https://doi.org/10.25967/370094.

[3] Benad, J., and Vos, R., "Design of a Flying V Subsonic Transport," *ICAS Proceedings*, 2022. URL https://www.icas.org/ICAS_ARCHIVE/ICAS2022/data/preview/ICAS2022_0358.htm.

[4] Faggiano, F., Vos, R., Baan, M., and van Dijk, R., "Aerodynamic Design of a Flying V Aircraft," *17th AIAA Aviation Technology, Integration, and Operations Conference*, 2017. https://doi.org/10.2514/6.2017-3589.

[5] Palermo, M., and Vos, R., "Experimental Aerodynamic Analysis of a 4.6%-Scale Flying-V Subsonic Transport," *AIAA SciTech Forum*, 2020. https://doi.org/10.2514/6.2020-2228.

[6] Cappuyns, T., *Handling Qualities of a Flying V Configuration*, MSc Thesis, Delft University of Technology, 2019. URL http://resolver.tudelft.nl/uuid:69b56494-0731-487a-8e57-cec397452002.

[7] Joosten, S., Stroosma, O., Vos, R., and Mulder, M., "Simulator Assessment of the Lateral-Directional Handling Qualities of the Flying-V," *AIAA SciTech Forum*, National Harbor, MD, 2023. https://doi.org/10.2514/6.2023-0906.

[8] Torelli, R., Stroosma, O., Vos, R., and Mulder, M., "Piloted Simulator Evaluation of Low-Speed Handling Qualities of the Flying-V," *AIAA SciTech Forum*, National Harbor, MD, 2023. https://doi.org/10.2514/6.2023-0907.

[9] Vugts, G., Stroosma, O., Vos, R., and Mulder, M., "Simulator Evaluation of Flightpath-oriented Control Allocation for the Flying-V," *AIAA SciTech Forum*, 2023. https://doi.org/10.2514/6.2023-2508.

[10] van Overeem, S., Wang, X., and van Kampen, E.-J., "Modelling and Handling Quality Assessment of the Flying-V Aircraft," *AIAA SciTech Forum*, San Diego, CA, 2022. https://doi.org/10.2514/6.2022-1429.

[11] van Overeem, S., Wang, X., and van Kampen, E.-J., "Handling Quality Improvements for the Flying-V Aircraft using Incremental Nonlinear Dynamic Inversion," *AIAA SciTech Forum*, National Harbor, MD, 2023. https://doi.org/10.2514/6.2023-0105.

[12] Stougie, J., Pollack, T., and van Kampen, E.-J., "Incremental Nonlinear Dynamic Inversion control with Flight Envelope Protection for the Flying-V," *AIAA SciTech Forum*, Orlando, FL, 2024. https://doi.org/10.2514/6.2024-2565.

[13] Huang, Y., Zhang, Y., Pool, D. M., Stroosma, O., and Chu, Q., "Time-Delay Margin and Robustness of Incremental Nonlinear Dynamic Inversion Control," *Journal of Guidance, Control, and Dynamics*, Vol. 45, No. 2, 2022, pp. 394–404. https://doi.org/10.2514/1.G006024.

[14] Di Francesco, G., and Mattei, M., "Modeling and Incremental Nonlinear Dynamic Inversion Control of a Novel Unmanned Tiltrotor," *Journal of Aircraft*, Vol. 53, No. 1, 2016, pp. 73–86. https://doi.org/10.2514/1.C033183.

[15] Sieberling, S., Chu, Q. P., and Mulder, J. A., "Robust Flight Control Using Incremental Nonlinear Dynamic Inversion and Angular Acceleration Prediction," *Journal of Guidance, Control, and Dynamics*, Vol. 33, No. 6, 2010, pp. 1732–1742. https://doi.org/10.2514/1.49978.

[16] Wang, X., van Kampen, E.-J., Chu, Q., and Lu, P., "Stability Analysis for Incremental Nonlinear Dynamic Inversion Control," *Journal of Guidance, Control, and Dynamics*, Vol. 42, No. 5, 2019, pp. 1116–1129. https://doi.org/10.2514/1.G003791.

[17] Field, E., "The application of a C* flight control law to large civil transport aircraft," Tech. rep., College of Aeronautics, Cranfield Institute of Technology, Cranfield, England, UK, 1993. URL https://dspace.lib.cranfield.ac.uk/handle/1826/186.

[18] Tekles, N., Chongvisal, J., Xargay, E., Choe, R., Talleur, D. A., Hovakimyan, N., and Belcastro, C. M., "Design of a Flight Envelope Protection System for NASA's Transport Class Model," *Journal of Guidance, Control, and Dynamics*, Vol. 40, No. 4, 2017, pp. 863–877. https://doi.org/10.2514/1.G001728.

[19] Stroosma, O., van Paassen, M. M., and Mulder, M., "Using the SIMONA Research Simulator for Human-machine Interaction Research," *AIAA Modeling and Simulation Technologies Conference and Exhibit*, 2003. https://doi.org/10.2514/6.2003-5525.

[20] Cooper, G. E., and Harper, R. P., "The Use of Pilot Rating in the Evaluation of Aircraft Handling Qualities," Tech. rep., NASA Ames Research Center, 4 1969. URL https://ntrs.nasa.gov/citations/19690013177.

[21] "AC 25-7D, Flight Test Guide for Certification of Transport Category Airplanes," Tech. rep., U.S. Department of Transportation, Federal Aviation Administration, 2018. URL https://www.faa.gov/documentLibrary/media/Advisory_Circular/AC_25-7D.pdf.

[22] "Easy Access Rules for Large Aeroplanes (CS-25)," Tech. rep., European Union Aviation Safety Agency, 2022. URL https://www.easa.europa.eu/en/document-library/easy-access-rules/easy-access-rules-large-aeroplanes-cs-25.

[23] Ruiz Garcia, A., Vos, R., and de Visser, C., "Aerodynamic Model Identification of the Flying V from Wind Tunnel Data," *AIAA SciTech Forum*, Virtual Event, 2020. https://doi.org/10.2514/6.2020-2739.

[24] Lombaerts, T., Looye, G., Ellerbroek, J., and y Martin, M. R., "Design and Piloted Simulator Evaluation of Adaptive Safe Flight Envelope Protection Algorithm," *Journal of Guidance, Control, and Dynamics*, Vol. 40, No. 8, 2017, pp. 1902–1924. https://doi.org/10.2514/1.G002525.

[25] Durham, W., A. Bordignon, K., and Beck, R., *Aircraft Control Allocation*, John Wiley & Sons, Ltd, 2017. https://doi.org/10.1002/9781118827789.

[26] "Flying Qualities of Piloted Airplanes," Tech. rep., U.S. Military, 1980. URL http://everyspec.com/MIL-SPECS/MIL-SPECS-MIL-F/MIL-F-8785C_5295/.

[27] "Flying Qualities of Piloted Aircraft," Tech. rep., United States of America, Department of Defense, 1990. URL https://engineering.purdue.edu/~andrisan/Courses/AAE490F_S2008/Buffer/mst1797.pdf.

[28] Asaro, S., Atmaca, D., van Kampen, E.-J., and Vos, R., "Control Surface Allocation based on Offline Handling Quality Simulations for a Flying Wing Aircraft," *AIAA SciTech Forum*, Orlando, FL, 2025.

[29] H. H. Chen, J., and Vos, R., "Conceptual Design of a Piloted Quarter-Scale Flying-V Research Airplane," *AIAA SciTech Forum*, Orlando, FL, 2025.

[30] Asaro, S., and Vos, R., "Synthesis of the Aerodynamic Model of a Flying Wing Aircraft," *AIAA SciTech Forum*, Orlando, FL, 2025.